

## EXPERIMENTAL INVESTIGATION OF COMPRESSIBILITY EFFECTS IN AXISYMMETRIC SUPERSONIC EJECTORS AND FREE JETS

Kenneth Yi-Nian Hinh<sup>1</sup>, Robert J. Martinuzzi and Craig Johansen

Department of Mechanical and Manufacturing Engineering  
University of Calgary

2500 University Drive NW, Calgary, Alberta T2N 1N4, Canada

kenneth.hinh@ucalgary.ca, rmartinu@ucalgary.ca and johansen@ucalgary.ca

### ABSTRACT

Particle image velocimetry (PIV) measurements were conducted of supersonic free jets and supersonic entrainment ejectors configured as an axisymmetric compressible jet into a constant area circular duct. Flows from a primary nozzle designed for a Mach number of 1.25 were investigated at over, perfect and under expanded conditions. Measurements of the velocity and Reynolds stresses allowed for a characterization of the jet flow not previously reported for a compressible axisymmetric ejector. The compressibility effects in the free jet were found to be in accord with those observed for the compressible mixing layer, suppressing the growth rate and Reynolds stresses with the convective Mach number,  $M_c$ . Similarity analysis was performed on the compressible free jet, which indicated the conditions for self-preservation in the mean momentum equation which allowed for the collapse of the Reynolds shear stresses by the jet spreading rate and centerline velocity. In the ejector the velocity profiles collapsed with the jet excess velocity and the jet thickness, but the spreading rate itself function of the both compressibility and confinement. Instead, the Reynolds shear stresses were collapsed with  $\Phi(M_c)$ , which expresses the effects of compressibility through  $M_c$ .

### INTRODUCTION

The rapid development of low-orbit reusable vehicles motivates interest in high-speed impulse propulsion systems for aerospace applications. With few moving parts, ejector pumps are an attractive device to provide thrust augmentation for rockets, ramjets and gas turbines. The confined turbulent axisymmetric jet is a laboratory simplification allowing the study of compressibility effects on the turbulence. An understanding of these effects is important for characterizing mixing and entrainment ratios determining the performance of the ejector.

Earlier studies mostly focused on the compressible mixing layer, where compressibility is observed to have a stabilizing effect on turbulence and is most evident through the suppression of the Reynolds stresses and, as a result, the growth rate. The convective Mach number,  $M_c$ , is used to scale the compressibility effects and is the Mach number in the frame of reference of the convective speed of coherent motions between the inner and outer flows (Papamoschou & Roshko, 1988).

The vorticity thickness,  $\delta'_\omega$ , is typically used to characterize the compressible mixing layer (Dimotakis, 1991) and is

defined by:

$$\frac{1}{\delta'_\omega} = \frac{1}{\Delta U} \left[ \frac{d\bar{u}(y)}{dy} \right]_{max} \quad (1)$$

where  $\Delta U$  is the velocity difference across the layer,  $\bar{u}(y)$  is the mean velocity and  $y$  the transverse distance. The modification on the vorticity thickness growth rate due to compressibility through the convective Mach number is expressed the relationship,

$$\delta'_\omega = \delta'_0 \Phi(M_c) \quad (2)$$

where  $\delta'_0$  and  $\delta'_\omega$  is the change of the vorticity thickness in the streamwise direction for the incompressible and compressible cases, respectively, and  $\Phi(M_c)$  is determined empirically. The single prime represents a spatial derivative. A function fitted from experimental data to represent  $\Phi(M_c)$  is given by Dimotakis (1991),

$$\Phi(M_c) = 0.8 \exp[-3M_c^2] + 0.2 \quad (3)$$

Barre *et al.* (1994) suggests that in the mixing layer, the Reynolds shear stress is also related to  $\delta'_\omega$  by,

$$\frac{-\overline{u''v''}}{(\Delta U)^2} \max = \frac{1}{2} K(s, q, M_c) \delta'_\omega \quad (4)$$

where  $K(s, q, M_c)$  is typically described as an eddy diffusivity time, which represents the growth rates of the eddies in a convected coordinate system and is determined empirically. The ratios,  $s$  and  $q$ , denote the ratio between the low speed and high speed sides for density and velocity respectively. The double prime denotes the temporal fluctuations and the over bar the temporal averaging.

Beside the geometrical differences between the mixing layer and the axisymmetric jet, the jet convective Mach number is a function of the streamwise distance,  $x$ , as the centerline velocity of the jet decays and in the confined jet, the secondary flow is entrained. In the incompressible confined jet the mean velocity profiles exhibit similarity when written in the form (Razinsky & Brighton, 1971),

$$f(\eta) = \frac{\bar{u} - \bar{U}_2}{\bar{u}_m - \bar{U}_2} = \frac{\bar{U}}{\bar{U}_m} \quad (5)$$

<sup>1</sup>Corresponding author

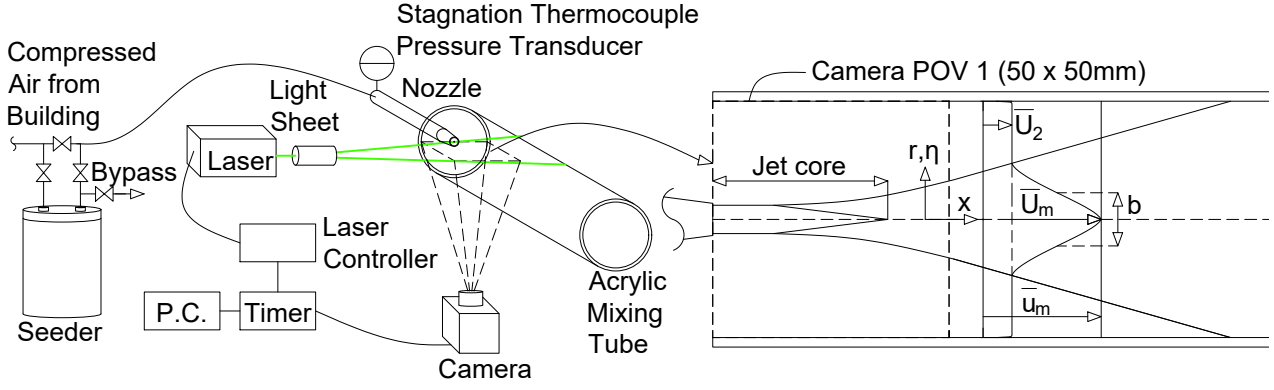


Figure 1: Schematic of experimental setup and nomenclature for velocities for the confined jet scenario. In the free jet,  $U_2 = 0$  and the acrylic mixing tube is omitted.

Whereas the vorticity thickness,  $\delta_\omega$ , is used to describe the thickness in the compressible mixing layers, the radius at half the maximum excess velocity,  $b$ , is typically used to collapse jet profiles with  $\eta = r/b$ . By construction,  $b$  and  $\delta_\omega$  and their evolution are proportional for self-similar flows. The velocity difference across the shear layer is considered to be the excess mean centerline jet velocity  $\bar{U}_m$  and the excess mean velocity,  $\bar{U}$  are calculated as the difference of the mean flow  $\bar{u}$  and the secondary flow velocity  $\bar{U}_2$ .  $\bar{u}_m$  is the maximum of the mean flow occurring at  $\eta = 0$ . For the free jet,  $\bar{U}_2 = 0$ .

Investigations on the local effects of compressibility on jets are limited. Schadow *et al.* (1990) employed total pressure measurements and Schlieren photography to determine the overall spreading rate in coaxial jets. The effect on jet swirl on the entrainment of the jet was investigated by Naughton *et al.* (1997) and the growth rate was determined from planar laser scattering (PLS) measurements. In these cases, the spreading rates were found to be suppressed by  $M_c$ , but since measurements were taken at a limited number of axial positions, the effect of  $M_c$  on the local spreading rate and its implications on the similarity of the jet not been investigated.

Using particle image velocimetry (PIV), a full field measurement is possible to investigate the effects of  $M_c$  on the spreading rate at a high resolution. In this case, the primary jet has a convective Mach number is  $M_{cm} = (\bar{u}_m - U_c)/a_1$  and for the secondary flow,  $M_{c2} = (U_c - \bar{U}_2)/a_2$ . The convective Mach number is taken to be a weighted average of the convective Mach numbers for the high speed side and low speed side of the shear layer, therefore  $M_c = \sqrt{M_{cm}M_{c2}}$ . Here  $a_m$  and  $a_2$  are the speeds of sound of the jet and secondary flow respectively. The convective velocity,  $U_c$  of the large structures in shear layer is given by,

$$U_c = \frac{a_2\bar{u}_m + a_1\bar{U}_m}{a_1 + a_2} \quad (6)$$

In this investigation, the local relationship between  $M_c$ , and the suppression of the vorticity thickness growth rate,  $\delta'_\omega$ , for the free jet was found to behave similarly to the mixing layer and is compared to other literature findings. For clarity, the jet growth rate  $b'$  is confirmed to be proportional to  $\delta'_\omega$ . In the mixing layer, by scaling the compressibility effects through the vorticity thickness growth of the shear layer, similarity is observed, and was shown that the compressibility effects are absorbed into the spreading rate and do not have an effect on the velocity profiles themselves (Menaar, 2003).

From the theory of incompressible jets, George (1988) argues that self-preservation of the mean momentum equations is possible when the Reynolds shear stress scales proportionally to the jet thickness growth rate, departing from the classical theory where  $b$  must be proportional to  $x$ . In the present work, similarity arguments are investigated for the free compressible jet and shows that the Reynolds shear stress scaling can be extended to the compressible scenario when  $M_c$  effects the spreading rate proportionally to the Reynolds shear stress. Experimental measurements of the evolution of the spreading rate, velocities and Reynolds stresses influenced by  $M_c$  as the jet develops shows this is the case in the free compressible jet. In the confined scenario, when scaled by local variables, the velocity profiles and shear Reynolds stress profiles collapse onto a single curve suggesting self-similarity.

## EXPERIMENTAL SETUP

The experimental setup is shown schematically in Fig. 1 along with a definition sketch and nomenclature. Planar PIV was used to measure two-component velocity fields in the plane bisecting the center axis of the mixing tube within a supersonic ejector. The streamwise position of the measurements begin where the exit plane of the nozzle and the entrance of the mixing tube coincide. A Mach 1.25 primary jet with an exit diameter of  $d = 6.35$  mm was investigated. Pressure ratios,  $P/P_{stag}$ , of 0.3378, 0.3890 and 0.4343 resulting in over, perfect and under expanded conditions, respectively, were investigated.

The mixing tube is cast acrylic ( $D = 54$  mm,  $l = 914.4$  mm) and the stagnation temperature upstream of the jet was measured to be 295.15K. Planar measurements in the window spanned the entire diameter of the mixing tube from a streamwise to nozzle diameter ratio ( $x/d$ ) of 0 to 25 are patched from four contiguous fields-of-view. The nozzle and the mixing tube were mounted on rails which slide independently of the laser and the camera in the streamwise direction, ensuring that the position of the light sheet in respect to the camera is identical between measurements. Contiguous field-of-views overlap 10.8 mm in the streamwise direction.

Both the ambient air and the jet were seeded with  $1 \mu\text{m}$  Di-Ethyl-Hexyl-Sebacat (DEHS) from a six-jet Laskin nozzle (TSI 9307-6). Ragni *et al.* (2011) showed that the particle response time for DEHS of this size is approximately  $\tau_p = 2\mu\text{s}$  which was sufficiently low to allow a resolution of the velocity fluctuations and gradients in this flow.

The PIV consisted of a CMOS camera with a sensor size

of  $20 \times 20 \mu\text{m}$  (*FastCAM* Photron SA-5) and a resolution of  $1024 \times 1024$ . The camera was equipped with a *Nikon* AF Micro-Nikkor 60 mm  $f/2.8D$  lens and was mounted perpendicular 20 cm from to the light sheet. A third-order polynomial spatial calibration was performed before each test to correct for any distortions from imaging through the acrylic mixing tube wall. The camera inter-frame time is  $0.23 \mu\text{s}$  and is independent of frame rate and resolution. Rhodamine 6G based paint was applied on the interior surface of the mixing tube, combined with a band-pass optical filter, nearly eliminating internal reflections.

The illumination source was a dual cavity Nd:YLF laser (*Photonics* DM20-527-DM) with a repetition rate up to 10 kHz with a maximum laser energy of 20 mJ per pulse. A 1 mm thick light sheet was formed from two spherical lenses and a cylindrical lens. Measurements were conducted in dual-pulse mode with a separation interval of 1 to  $1.5 \mu\text{s}$  to ensure that the particles moved about 7 pixels at the center of the jet between image pairs. A silicon photodetector (*Thorlabs* DET02AFC) was used to ensure that the pulse separation time matches the time sent by the trigger.

Image pairs were collected and processed using *LaVision* DaVis 10.2.0 PIV software. Each test consisted of 1000 image pairs, with the Reynolds stresses converging after approximately 750 pairs. Processing was done using a multi-pass strategy resulting in a vector field with  $32 \times 32$  pixel window size with 75% overlap. This provided about 20 vectors across the jet exit diameter.

## RESULTS AND DISCUSSION

In this study, the local convective Mach number  $M_c$  was calculated at each streamwise position with the jet centerline velocity as  $\bar{u}_m$  and the secondary flow velocity as  $\bar{U}_2$ , with  $a_2 = 342 \text{ m/s}$ , calculated from a temperature of 291.15 K. As jet temperature measurements were not available,  $a_1$  was approximated by averaging the temperature of the ambient flow and jet exit static temperature calculated from isentropic relations.

The governing equations in this region of flow are those of conservation of mass and momentum and the momentum

integral.

$$\frac{1}{r} \frac{\partial(\bar{\rho} \bar{v} r)}{\partial r} + \frac{\partial(\bar{\rho} \bar{u})}{\partial x} = 0 \quad (7)$$

$$\bar{\rho} \bar{u} \frac{\partial \bar{u}}{\partial r} + \bar{\rho} \bar{v} \frac{\partial \bar{u}}{\partial x} = -\frac{1}{r} \frac{\partial(\bar{\rho} \overline{u'v'})}{\partial r} \quad (8)$$

$$M_0 = 2\pi \int_0^\infty \bar{\rho} \bar{u}^2 r dr \quad (9)$$

Note that the velocity-density correlations are assumed to be small and thus omitted from the momentum equation. This is essentially Morkovin's hypothesis, which is typically valid in free shear flows with  $M_c$  less than 1.5 (Bradshaw, 1977). The shape function for the density profile,  $g(\eta)$  is not universal, and is a function of  $s$  and  $q$  through the Crocco-Busemann relations. The Reynolds shear stress is represented by its maximum value,  $R_s$ , and a shape function,  $h_{12}$ . Performing a similarity analysis following George (1988), the functional dependencies of  $\bar{U}_m$ ,  $\bar{\rho}_s$ ,  $R_s$  and  $b$  are left remain determined. For the compressible free jet:

$$\bar{U} = \bar{U}_m f(\eta) \quad (10)$$

$$\bar{\rho} = \bar{\rho}_s g(\eta; s, q) \quad (11)$$

$$-\overline{u'v'} = R_s h_{12}(\eta) \quad (12)$$

$$\eta = r/b \quad (13)$$

In the free jet, the jet momentum,  $M_0$ , is assumed to be constant. From (9), the relationship between the density, centerline velocity and jet spreading rate is,

$$\bar{U}_m = B \left( \frac{M_0}{\bar{\rho}_s} \right)^{1/2} b^{-1} \quad (14)$$

where  $B$  is a constant. Upon substitution of (11)-(13) into (8)-(9), the mean-momentum equation is:

$$\left[ \frac{1}{2} \frac{\bar{\rho}'_m}{\bar{\rho}_m} \right] \left( g f^2 - \frac{(g f)'}{g \eta} \int_0^\eta g f \bar{\eta} d\bar{\eta} \right) - \left[ \frac{b'}{b} \right] \left( g f^2 + \frac{(g f)'}{g \eta} \int_0^\eta g f \bar{\eta} d\bar{\eta} \right) = \left[ \frac{R_s}{b \bar{U}_m^2} \right] \frac{(\eta g h_{12})'}{\eta} \quad (15)$$

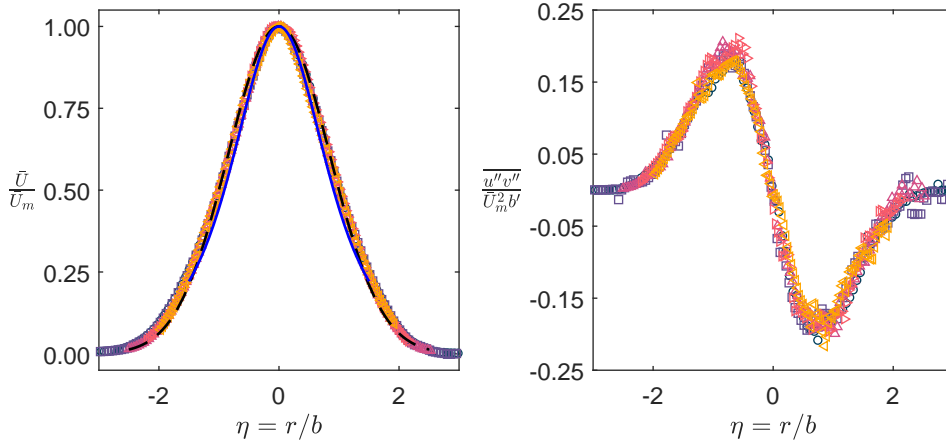


Figure 2: The velocity profile (left) with overlay of Gaussian shape function,  $f(\eta) = e^{-\ln(2)\eta^2}$  (---) and Schlichting's jet equation with constant eddy viscosity  $f(\eta) = (1 + \eta^2/2)^{-2}$  (—). The Reynolds shear stress (right) for perfectly expanded free jet. Axial positions  $x/d = 12.5$  ( $\circ$ );  $15.0$  ( $\square$ );  $17.5$  ( $\triangle$ );  $20.0$  ( $\triangleleft$ );  $22.5$  ( $\triangleright$ ).

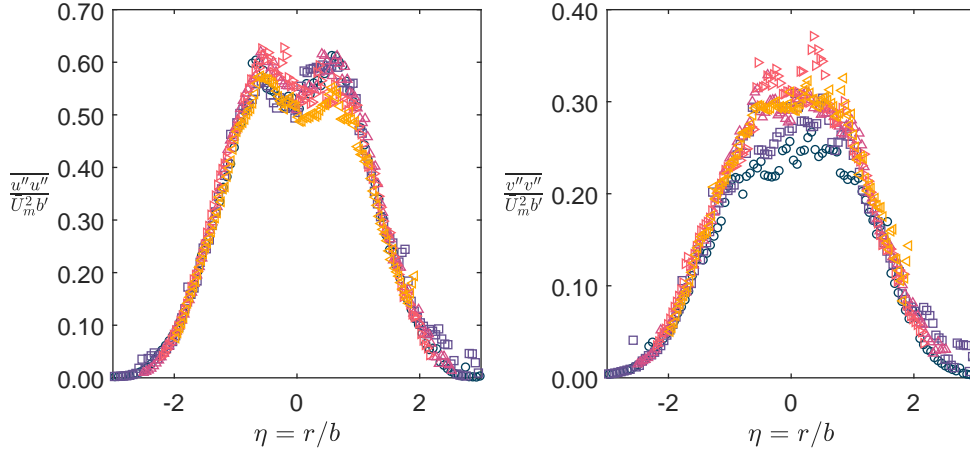


Figure 3: Reynolds normal streamwise (left) and transverse (right) stresses for the perfectly expanded free jet. Axial positions  $x/d = 12.5$  ( $\circ$ );  $15.0$  ( $\square$ );  $17.5$  ( $\triangle$ );  $20.0$  ( $\triangleleft$ );  $22.5$  ( $\triangleright$ ).

The first term in (15) differs from the incompressible free jet and, if large, needs to be considered if similarity conditions are to be satisfied. However, in the present flow, this term may be assumed negligible. Examining the shape functions, the first term consists of a difference between two even functions, in contrast to a sum in the second term. In most cases, the shape functions are the same order of magnitude, thus the first term is small when compared to the second.

In jets, the centerline temperature, and through the ideal gas law the density, diffuses to ambient conditions and approaches unity as the jet develops. If the density ratio can be considered nearly constant, the shape function  $g(\eta)$  becomes a constant function. For these conditions, the equation of George (1988) is recovered.

$$-f^2 - \frac{f'}{\eta} \int_0^\eta f \bar{\eta} d\bar{\eta} = \left[ \frac{R_s}{\bar{U}_m^2 b'} \right] \frac{(\eta h_{12})'}{\eta} \quad (16)$$

The foregoing analysis has implications for the characteristics in compressible jets. If the effects of the shape function  $g(\eta)$  can be neglected, the velocity profiles are expected to resemble the incompressible scenario as long as the first term in (15) remains small and that the compressibility effects are not expressed in the scaled velocity profiles themselves but through the growth rate of the jet. In Fig. 2, the velocity profile agrees with two common functions used to represent free incompressible jets, indicating that at the current jet conditions,  $g(\eta)$ , has a small effect.

George (1988) hypothesizes for self-preservation of the mean momentum equation, the quantities  $\bar{U}_m$ ,  $R_s$  and  $b'$  must maintain the same relative balance at the same relative locations. In the incompressible jet, this explained the effect of initial conditions on the self-preservation. In the current case, this can be extended to determine the effect of compressibility on self-preservation for the compressible jet.

The incompressible free jet is expected to grow linearly within the similarity region. Thus, any change in the growth rate in the compressible scenario is due to the effect of  $M_c$ . The relationship between the convective Mach number and the jet thickness growth rate, recalling that  $b' \sim \delta'_\omega$  and shown in Fig. 4, agrees well with the function from (3). This shows that locally, the vorticity thickness growth rate in compressible free jets behaves like the mixing layer counterpart. For comparison,

the vorticity thickness is scaled 0.142, which is the value for a free incompressible jet from experiments by Moore (1977).

From (16), self-preservation of the mean momentum equation of the free jet requires that the streamwise variation of  $b'$  be proportional to  $R_s/\bar{U}_m^2$ . As the evolution of  $\delta_\omega$  and  $b'$  is proportional,  $b'$  is similarly modified by  $\Phi(M_c)$  and thus  $R_s/\bar{U}_m^2$  must also be altered by  $M_c$  in the same way. In Fig. 5, the normalized maximum Reynolds shear stress,  $R_s/\bar{U}_m^2$ , is plotted against  $M_c$  and appears to be similarly modified by  $\Phi(M_c)$  for comparison, the relation for  $\Phi(M_c)$  from Dimotakis (1991), multiplied by 0.02 is also shown. The modification is similar to that for the compressible mixing layer where the Reynolds shear stress is modified with  $\Phi(M_c)$  (Goebel & Dutton, 1991).

The relationship between  $\bar{U}_m$ ,  $R_s$  and  $b'$  in (16) in the jet literature is referred to as an amplification factor, but perhaps the analogue from the compressible mixing layer, the eddy diffusivity time,  $K(s, q, M_c)$ , introduced in (4) which has a

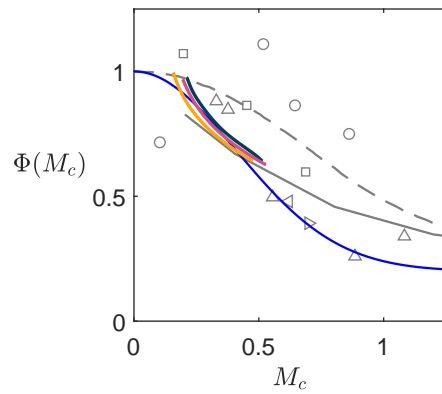


Figure 4: Vorticity thickness growth rate suppression. Experimental results in markers: Papamoschou & Roshko (1988) ( $\triangle$ ); Samimy & Elliott (1990) ( $\circ$ ); Goebel & Dutton (1991) ( $\square$ ); Barre *et al.* (1994) ( $\triangleleft$ ); Naughton *et al.* (1997) ( $\triangleright$ ). Mixing Layer DNS in black lines: Freund *et al.* (2000) ( $- -$ ); Matsuno & Lele (2020) ( $-$ ). Relation from Dimotakis (1991) ( $-$ ); Current investigation of Mach 1.25 free jets: Under expanded ( $-$ ), Perfectly expanded ( $-$ ), Over expanded ( $-$ )

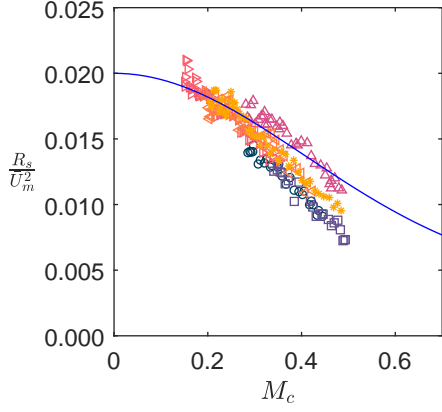


Figure 5: Suppression of maximum Reynolds shear stresses with increasing convective Mach number. Only includes region where the velocity profile is self-similar. Free: Under expanded (\*); Perfectly expanded (<); Over expanded (>). Confined: Under expanded (Δ); Perfectly expanded (□); Over expanded (○). Relation from Dimotakis (1991) now multiplied by 0.02 (—)

similar form, is more appropriate. To differentiate from the mixing layer, the eddy diffusivity time for the jet is:

$$K_{\text{jet}} = \frac{R_s}{\bar{U}_m^2 b'} \quad (17)$$

Fig. 6 shows  $K_{\text{jet}}$  as a function of  $x/d$ . The observation that  $K_{\text{jet}}$  is nearly constant is then consistent with the assumption that the suppression of  $b'$  and  $R_s$  due to compressibility can be expressed as  $b' = \Phi(M_c)b'_0$  and  $R_s = \Phi(M_c)R_{s,0}$ , where the subscript, 0, indicates the value in the incompressible case. A constant  $K_{\text{jet}}$  as the jet develops suggests that the flow is self-preserving to at least the mean momentum equation. Satisfying this condition results in the Reynolds shear stress collapsing onto a single curve when scaled by  $\bar{U}_m^2 b'$  as shown in Fig. 2.

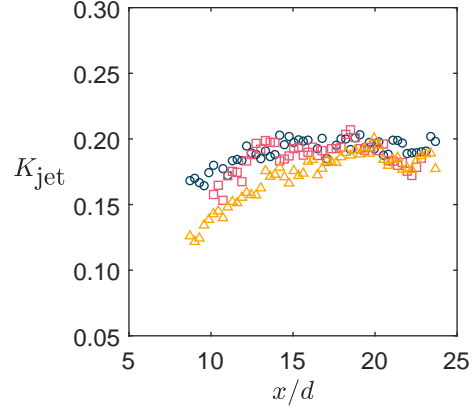


Figure 6: Jet eddy diffusivity time,  $K_{\text{jet}}$ , for the free jet. Over expanded (Δ); Perfectly expanded (□); Under expanded (○).

The behavior of  $K_{\text{jet}}$  due to compressibility can be explained by analogy to the mixing layer eddy diffusivity time,  $K(s, q, M_c)$ . Mena (2003) found that  $K(s, q, M_c)$  is relatively constant, but especially when the density ratio is near unity.

In the confined jet, the confinement introduces a secondary flow, momentum loss and pressure gradient and as a consequence, the flow is not self-preserving in the mean momentum equation and  $K_{\text{jet}}$  is not constant. The velocity profiles collapse when scaled by the excess velocity, and is nearly identical to the free jet profile with some deviation at the edges of the jet. In Fig. 5, the suppression of the Reynolds shear stress due to compressibility is still captured by  $\Phi(M_c)$ , suggesting that the Reynolds shear stress can be collapsed by normalizing by  $\bar{U}_m^2 \Phi(M_c)$ , as shown in Fig. 7. This indicates that the effects of confinement and compressibility can be quantified through the local variables,  $\bar{U}_m$ ,  $M_c$ , and  $b$ , making this flow self-similar.

Due to the confinement, the incompressible spreading rate is generally no longer constant and is unknown, and without a method of normalizing  $b'$ ,  $\Phi(M_c)$  cannot be determined from the confined experimental results. Although this is the case, as the Reynolds shear stress is suppressed through  $\Phi(M_c)$ ,

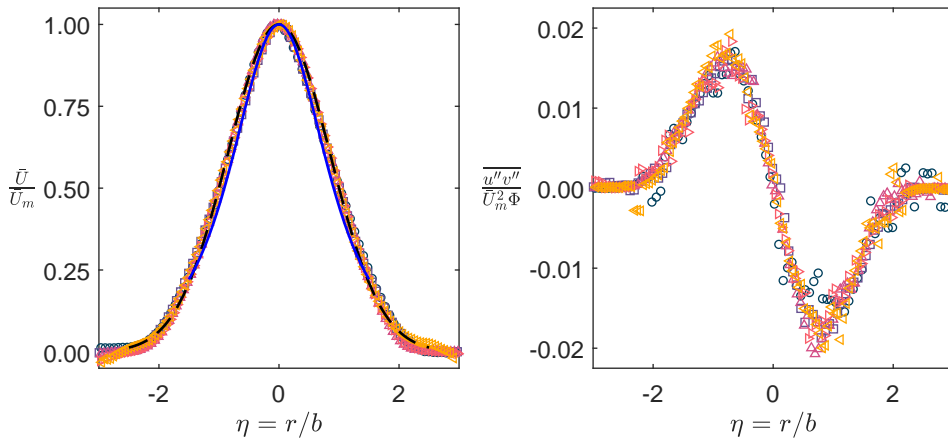


Figure 7: The velocity profile (left) with overlay of Gaussian shape function,  $f(\eta) = e^{-\ln(2)\eta^2}$  (---) and Schlichting's jet equation with constant eddy viscosity  $f(\eta) = (1 + \eta^2/2)^{-2}$  (—). The Reynolds shear stress (right) for supersonic ejector with primary jet Mach number = 1.25. Axial positions  $x/d = 12.5$  (○); 14.125 (□); 15.75 (Δ); 17.375 (<); 19.0 (>).

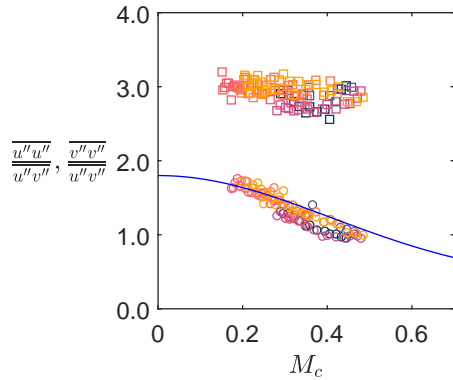


Figure 8: Reynolds stress anisotropy with  $M_c$ . Ratios of maximum Reynolds stresses.  $\overline{u''u''}/\overline{u''v''}$ , Free: Under expanded ( $\square$ ); Perfectly expanded ( $\square$ ); Over expanded ( $\square$ ), Confined: Under expanded ( $\square$ ); Perfectly expanded ( $\square$ ); Over expanded ( $\square$ ).  $\overline{v''v''}/\overline{u''v''}$ , (o); Perfectly expanded, (o); Over expanded (o), Confined: Under expanded (o); Perfectly expanded (o); Over expanded (o). Relation from Dimotakis (1991) now multiplied by 1.8 (—)

the spreading rate is also expected to remain modified through  $b' = \Phi(M_c)b'_0$ .

The anisotropy of the Reynolds stresses is illustrated in Fig. 8. Although anisotropy is expected, there remains disagreement as to how the stresses are affected by  $M_c$ . The streamwise Reynolds stress,  $\overline{u''u''}$ , in some studies was found to be unaffected by  $M_c$  (Goebel & Dutton, 1991; Freund *et al.*, 2000) but was found to be suppressed with  $M_c$  in others (Elliott & Samimy, 1990; Samimy & Elliott, 1990; Matsuno & Lele, 2020). In the compressible free and confined jet, the streamwise Reynolds stress was found to agree with the latter case. As indicated in squares in Fig. 8, the constant ratio implies that the Reynolds transverse and shear stress are suppressed similarly by  $M_c$ . Unlike studies in the mixing layer, the transverse stress ratio  $\overline{v''v''}/\overline{u''v''}$  shows stronger suppression with  $M_c$  than the streamwise and shear stresses.

## CONCLUSION

The compressible shear layer within the supersonic free jets and axisymmetric supersonic ejector and of Mach number 1.25 was investigated with particle image velocimetry (PIV), providing a detailed measurement of the turbulent stresses and jet thickness growth rate as the jet developments, which allowed for an investigation relating the convective Mach number,  $M_c$ , to the Reynolds stresses and spreading rate at each streamwise position of the jet. Similarity analysis introduced a condition for self-preservation in the mean momentum equation for the free compressible jet, where the eddy diffusivity time for the jet,  $K_{jet}$ , must be constant. In the ejector, the velocity and Reynolds shear stress collapsed with local variables as  $b'$  is a function of the confinement and the compressibility. Through the modification of  $R_\xi$  with  $\Phi(M_c)$ , the spreading rate is expected to also be suppressed with  $M_c$ .

## ACKNOWLEDGEMENTS

Funding for this work was provided by the Natural Sciences Engineering Research Council (NSERC) of Canada and Atlantis Research Labs Inc. through a Collaborative Research and Development (CRD) grant.

## REFERENCES

- Barre, S., Quine, C. & Dussauge, J. P. 1994 Compressibility Effects on the Structure of Supersonic Mixing Layers: Experimental Results. *Journal of Fluid Mechanics* **259**, 47–78.
- Bradshaw, P. 1977 Compressible Turbulent Shear Layers. *Annual Review of Fluid Mechanics* **9** (1), 33–52.
- Dimotakis, P. E. 1991 Turbulent Free Shear Layer Mixing and Combustion. *Progress in Astronautics and Aeronautics* **135** (Chapter 5), 76.
- Elliott, G. S. & Samimy, M. 1990 Compressibility Effects in Free Shear Layers. *Physics of Fluids A: Fluid Dynamics* **2** (7), 1231–1240.
- Freund, J. B., Lele, S. K. & Moin, P. 2000 Compressibility Effects in a Turbulent Annular Mixing Layer. Part 1. Turbulence and Growth Rate. *Journal of Fluid Mechanics* **421**, 229–267.
- George, W. K. 1988 The Self-Preservation of Turbulent Flows and Its Relation to Initial Conditions and Coherent Structures. *Advances in Turbulence* pp. 39–73.
- Goebel, S. G. & Dutton, J. C. 1991 Experimental Study of Compressible Turbulent Mixing Layers. *AIAA Journal* **29** (4), 538–546.
- Matsuno, K. & Lele, S. K. 2020 Compressibility Effects in High Speed Turbulent Shear Layers – Revisited. In *AIAA Scitech 2020 Forum*. Orlando, FL: American Institute of Aeronautics and Astronautics.
- Menaa, M. 2003 Density and Compressibility Effects on the Structure of Supersonic Mixing Layer. In *12th AIAA International Space Planes and Hypersonic Systems and Technologies*. Norfolk, Virginia: American Institute of Aeronautics and Astronautics.
- Moore, C. J. 1977 The Role of Shear-Layer Instability Waves in Jet Exhaust Noise. *Journal of Fluid Mechanics* **80** (2), 321–367.
- Naughton, J. W., Cattafesta III, L. N. & Settles, G. S. 1997 An Experimental Study of Compressible Turbulent Mixing Enhancement in Swirling Jets. *Journal of Fluid Mechanics* **330**, 271–305.
- Papamoschou, D. & Roshko, A. 1988 The Compressible Turbulent Shear Layer: An Experimental Study. *Journal of Fluid Mechanics* **197**, 453–477.
- Ragni, D., Schrijer, F., van Oudheusden, B. W. & Scarano, F. 2011 Particle Tracer Response Across Shocks Measured by PIV. *Experiments in Fluids* **50** (1), 53–64.
- Razinsky, E. & Brighton, J. A. 1971 Confined Jet Mixing for Nonseparating Conditions. *Journal of Basic Engineering* **93** (3), 333–347.
- Samimy, M. & Elliott, G. S. 1990 Effects of Compressibility on the Characteristics of Free Shear Layers. *AIAA Journal* **28** (3), 439–445.
- Schadow, K. C., Gutmark, E. & Wilson, K. J. 1990 Compressible Spreading Rates of Supersonic Coaxial Jets. *Experiments in Fluids* **10-10** (2-3), 161–167.